


## *Zitterbewegung* of Dirac quasiparticles emerged in a Su-Schrieffer-Heeger lattice

Yue Hu(胡玥), Zheng-Xin Guo(郭政鑫), Ze-Ming Zhong(钟泽明), Zhi Li(李志)

Chin. Phys. B . 2020, 29(11): 110302 . **doi:** 10.1088/1674-1056/abb45b
Journal homepage: http://cpb.iphy.ac.cn; http://iopscience.iop.org/cpb

**What follows is a list of articles you may be interested in**

---

## Exact solution of the (1+2)-dimensional generalized Kemmer oscillator in the cosmic string background with the magnetic field

Yi Yang(杨毅), Shao-Hong Cai(蔡绍洪), Zheng-Wen Long(隆正文), Hao Chen(陈浩), Chao-Yun Long(龙超云)

Chin. Phys. B . 2020, 29(7): 070302 . **doi:** 10.1088/1674-1056/ab888e

## Solution of the spin-one DKP oscillator under an external magnetic field in noncommutative space with minimal length

Bing-Qian Wang(王炳乾), Zheng-Wen Long(隆正文), Chao-Yun Long(龙超云), Shu-Rui Wu(吴淑蕊)

Chin. Phys. B . 2018, 27(1): 010301 . **doi:** 10.1088/1674-1056/27/1/010301

## Exact solution of the generalized Kemmer oscillator

Zi-Long Zhao(赵子龙), Chao-Yun Long(龙超云), Zheng-Wen Long(隆正文), Ting Xu(徐婷)

Chin. Phys. B . 2017, 26(8): 080301 . **doi:** 10.1088/1674-1056/26/8/080301

## Modes splitting in graphene-based double-barrier waveguides

Si-Pu You(有四普), Ying He(何英), Yan-Fang Yang(杨艳芳), Hui-Fang Zhang(张惠芳)

Chin. Phys. B . 2017, 26(3): 030301 . **doi:** 10.1088/1674-1056/26/3/030301

## Relativistic effect of pseudospin symmetry and tensor coupling on the Mie-type potential via Laplace transformation method

M. Eshghi, S. M. Ikhdair

Chin. Phys. B . 2014, 23(12): 120304 . **doi:** 10.1088/1674-1056/23/12/120304

---

# *Zitterbewegung* of Dirac quasiparticles emerged in a Su-Schrieffer–Heeger lattice*

Yue Hu(胡玥)[1], Zheng-Xin Guo(郭政鑫)[1], Ze-Ming Zhong(钟泽明)[1,2,†], and Zhi Li(李志)[1,‡]

[1] *Guangdong Provincial Key Laboratory of Quantum Engineering and Quantum Materials, Guangdong Provincial Engineering Technology Research Center for Quantum Precision Measurement, SPTE, South China Normal University, Guangzhou* 510006, *China*

[2] *School of Materials Science and Engineering, Guangdong Provincial Key Laboratory of Advanced Energy Storage Materials, South China University of Technology, Guangzhou* 510641, *China*

(Received 9 June 2020; revised manuscript received 23 July 2020; accepted manuscript online 2 September 2020)

We analytically and numerically investigate the dynamical properties of the tilted dispersion relativistic quasiparticles emerged in a cold atomic optical lattice system. By introducing the next nearest neighboring (NNN) hopping term into Su–Schrieffer–Heeger (SSH) model, the Dirac quasiparticles with tilted dispersion relation are realized. The results show that the tilted dispersion causes a drift in relativistic quasiparticles rather than affecting interference behavior between inner states. To be specific, the relativistic phenomena of the quasiparticles induced by the inner state interference (such as *Zitterbewegung*, Klein paradox, etc.) is completely unaffected by the tilted dispersion. In order to distinguish the drift induced by tilted dispersion and common initial velocity, we calculate the momentum distribution of the relativistic quasiparticles. We obtain the difference between the drift induced by initial velocity and tilted dispersion. The former affects the ZB, while the latter does not. By using this character, we propose a quench dynamics scheme to obtain a stable mono-spin state. The proposed cold atomic lattice system would provide a promising platform in exploring the intrinsic exotic physics of relativistic quasiparticles and the related systems.

**Keywords:** tilted dispersion, wave-packet dynamics, quantum quench

**PACS:** 42.50.Pq, 37.30.+i, 03.67.Bg, 76.30.Mi **DOI:** 10.1088/1674-1056/abb45b

## 1. Introduction

First predicted by Schrödinger in 1930,[1] *Zitterbewegung* (ZB) represents a spontaneous trembling movement of free relativistic particles with an extremely high frequency and small amplitude. Initially, the prediction was merely regarded as a theoretical fiction with its incredible oscillation amplitude ($A_{\rm ZB} = 10^{-12}$ m, the order of the Compton wavelength) and frequency ($\omega_{\rm ZB} = 10^{21}$ Hz) for a free electron. As technology advances, Gerritsma *et al*. finally realized the simulation of ZB phenomenon in a trapped ion system in 2010.[2] Our current exploration suggests that, far from being just unique to electrons, ZB is actually a universal phenomenon of multi-component relativistic quasiparticles, which reflects the interference between energy states.[3–7] Three conditions need to be satisfied to realize ZB phenomenon: first, a multiband system in which the interference can occur; second, energy bands which have opened gaps between them; third, a dispersion which satisfies odd power relationship, that is to say, energy–momentum relationship should satisfy $E = k^Z$, $Z = 1, 3, 5, \ldots$. We now exclude the case of higher order dispersion since it is hard to realize in condensed matter physics at present. The linear dispersion system satisfying the above conditions has been realized in many table-top experimental systems including graphene,[5] photonic crystals,[6] cold atomic lattice systems,[7] Weyl semimetals,[9,10] etc. The dynamics of quasiparticles in these systems has a common feature, i.e., satisfying the relativistic Dirac equation. Since the dynamic behavior of quasiparticles is good in judging the topological and transport characteristics of the system,[11] increasing attention has been paid to the dynamical behaviors of quasiparticles in various topological models (SSH model, Haldane model, Weyl semimetal, etc.). The Su–Schrieffer–Heeger (SSH) model[12] for polyacetylene, as the simplest one-dimensional topological model, describes spin-less fermions hopping on a one-dimensional lattice with staggered hopping amplitudes. In the past few years, SSH model has been investigated experimentally with ultra-cold atomic system,[13] photonic lattice,[14] and superconduction circuit.[15]

Over the past two decades, the manipulation of cold atoms has scored remarkable achievements.[11,16–22] Due to its high controllability and high purity, it has become one of the best quantum simulators. At present, the ultra-cold atomic op-

*Project supported by the National Key Research and Development Program of China (Grant Nos. 2016YFA0301803 and 2016YFA0302800), the National Natural Science Foundation of China (Grant Nos. 11604103, 11704132, 11822403, and 91636218), the NSAF, China (Grant Nos. U1801661 and U1830111), the PCSIRT, China (Grant No. IRT1243), the Natural Science Foundation of Guangdong Province, China (Grant Nos. 2016A030313436, 2018A030313322, and 2018A0303130066), the KPST of Guangzhou (Grant No. 201804020055), China Postdoctoral Science Foundation (Grant No. 2018M633063), and the Startup Foundation of SCNU.

†Corresponding author. E-mail: zhongzeming_scut@163.com

‡Corresponding author. E-mail: lizhi_nju@163.com

© 2020 Chinese Physical Society and IOP Publishing Ltd 

tical lattice system is widely used to simulate condensed matter physics and high-energy phenomena, especially those difficult to realize in traditional experiments, such as quantum phase transition,[16] quantum magnetic frustration,[23] nonlinear phenomena,[24–28] and the dynamic behavior of relativistic particles.[9,29–33] So far, cold atom systems can be used to simulate the relativistic dynamics that satisfies the Dirac/Weyl/Majorana equation by inducing the gauge potential and constructing the specific geometry of the optical lattice. As a result, Klein tunneling, ZB effect, and other relativistic dynamical phenomena have been realized successively in cold atomic systems.

In this paper, by introducing the next nearest neighboring (NNN) hopping term in the SSH model, we realize the relativistic quasiparticles with tilted dispersion and study the relevant dynamical properties. The paper is structured as follows. Section 2 introduces the ultracold atoms model and optical-lattice setup for simulating the Dirac quasiparticles' dynamics. The evolution of wavepacket dynamics is studied in Section 3 analytically and numerically. The analytical expression of momentum distribution is provided in Section 4. In Section 5, we propose a scheme of quench dynamics to realize component separation and pure mono-component state. Section 6 gives the conclusion.

## 2. Model

In order to realize SSH model with a tilted dispersion relation, we introduce the NNN hopping term to standard SSH model [see Fig. 1(a)]. The lattice can be formed by tunable retro-reflected laser beams of 780 nm and the hopping between sites can be tuned by laser-assisted transition technology. The corresponding tight-binding Hamiltonian reads

$$H = H_{\rm ssh} + H_{\rm tilt}, \tag{1}$$

with

$$H_{\rm ssh} = \sum_{n=1}^{N} \left\{ t_2(1+\alpha) a_n^{\dagger} b_n + t_2(1-\alpha) a_{n+1}^{\dagger} b_n + \text{h.c.} \right\}, \tag{2}$$

$$H_{\rm tilt} = \sum_{n=1}^{N} \left\{ \mathrm{e}^{\mathrm{i}\theta} t_1 (a_n^{\dagger} a_{n+1} + b_n^{\dagger} b_{n+1}) + \text{h.c.} \right\}, \tag{3}$$

where $a_n^{\dagger}$ ($b_n^{\dagger}$) and $a_n$ ($b_n$) are the creation and annihilation operators of cold atoms on $A$ ($B$) sublattice site, respectively, and $\theta$ is the hopping phase factor. Without loss of generality, we set $\theta = \pi/2$. In the model, $t_1$ and $t_2$ are the hopping amplitudes which connect the different $A$ ($B$) sublattice. The hopping amplitude in the unit cell is $t_2(1+\alpha)$ and that between two unit cells is $t_2(1-\alpha)$. By performing Fourier transform $a_n = \sum_k \mathrm{e}^{\mathrm{i}k_x \cdot na} a_k$ and $b_n = \sum_k \mathrm{e}^{\mathrm{i}k_x \cdot na} b_k$ (hereafter we set the lattice constant $a = 1$), we obtain the corresponding Bloch Hamiltonian

$$\begin{aligned} H(k) =& 2t_1 \sin k_x \sigma_0 - t_2(1-\alpha) \sin k_x \sigma_1 \\ &+ \left( 2\alpha t_2 + 2t_2(1-\alpha) \sin^2 \frac{k_x}{2} \right) \sigma_3, \end{aligned} \tag{4}$$

where $\sigma_i$ ($i = 0, 1, 3$) denote standard the Pauli matrices, which come from pseudospins of the $AB$ sublattices. To realize this model, it usually requires $PT$ combining symmetry. For the $\boldsymbol{k}$-space Hamiltonian [Eq. (4)], while the time-reversal symmetry and inversion symmetry are broken, the combining $PT$ symmetry remains intact. Since the dynamical properties of quasiparticles depend on the dispersion relationship near the degenerate point, the proximal band structure becomes the focus of our study. By considering $k_x = \boldsymbol{k} + q_x$, which is the displacement vector measured from $\boldsymbol{k}$ point, one can obtain the low-energy effective Hamiltonian

$$H_{\rm eff} = (v_0 \sigma_0 + v_x \sigma_1) q_x + mc^2 \sigma_3, \tag{5}$$

where $v_0 = 2t_1$ and $v_x = -t_2(1-\alpha)$ denote the Fermi velocity. $m = 2\alpha t_2$ is the effective mass and $c$ denotes the effective velocity of light. For simplify and without loss of generalization, hereafter we use $\hbar = c = 1$ in our calculation. The parameter $v_0$ plays the pivotal role in tilting the energy spectrum. The corresponding energy–momentum relation can be obtained as

$$E_q = v_0 q_x \pm \sqrt{v_x^2 q_x^2 + m^2}. \tag{6}$$

The energy–momentum relation with different $v_0$ is plotted in Fig. 1.

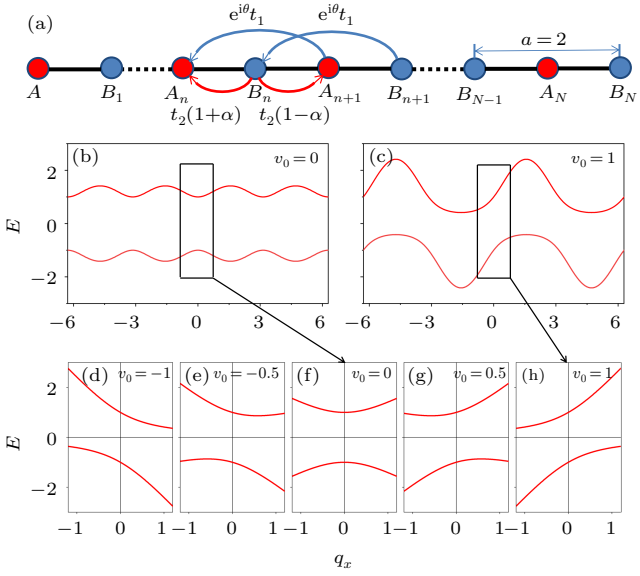



**Fig. 1.** (a) The proposed one-dimensional chain optical lattice scheme and atomic hopping configuration between the different $A$ (or $B$) sublattice sites. $t_1$ ($t_2$) denotes the hopping between sites of the same (different) type atoms, $a = 1$ is the lattice constant. $\theta = \pi/2$ is the hopping phase factor. (b) and (c) Dispersion relationship in the condition of Bloch Hamiltonian with $v_0 = 0$ and $v_0 = 1$, respectively. (d)–(h) Dispersion relationship with different $v_0$ in the condition of the low-energy effective Hamiltonian [Eq. (5)].

The corresponding dynamical properties of relativistic particles in the optical lattice can be described by the following equation:

$$\mathrm{i}\hbar\frac{\partial}{\partial t}\Psi = H_{\mathrm{eff}}\Psi. \tag{7}$$

## 3. The evolution of wave-packet dynamics

For studying the relativistic quasiparticles' wavepacket dynamics with different tilted dispersions, we directly solve the time-dependent Dirac equation [Eq. (7)]. In computation, we consider a general Gaussian wave packet

$$\Psi = (1/\sqrt{2\pi}L)^{1/2}\,\mathrm{e}^{\mathrm{i}q_0 x}\,\mathrm{e}^{-x^2/4L^2}\Phi, \tag{8}$$

as the initial state, where $\Phi = (c_1, c_2)^{\mathrm{T}}$ is the unit vector, T stands for matrix transposition, $L$ is the width of the wave packet, and $q_0$ is the wave vector. The corresponding wave function in momentum space is

$$\Psi_k = (L/\sqrt{\pi})^{1/2}\,\mathrm{e}^{-L^2(q_x-q_0)^2}\Phi. \tag{9}$$

Without loss of generality, we set $\Phi = \frac{1}{\sqrt{2}}(1,1)^{\mathrm{T}}$ and $q_0 = 0$. The visualized wavepacket evolution over time is plotted in Fig. 2.

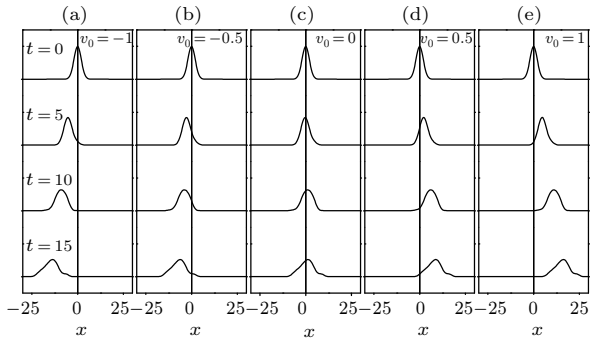



**Fig. 2.** (a)–(e) Numerically calculated probability distributions, $|\Psi(x,t)|^2$, with different time. The width of the initial wave packet $L = 2$, effective mass $m = 1$, effective light speed $v_x = 1$.

Figure 2(c) corresponds to the case of $v_0 = 0$, which is the standard one-dimensional Dirac quasiparticle. The wavepacket wiggles back and forth versus time, and soon develops ripples, which is the evidence of *Zitterbewegung*. Figures 2(a) and 2(b) [2(d) and 2(e)] exhibit the case $v_0 > 0$ ($v_0 < 0$). While the wavepacket exhibits the same instantaneous shape as the case of $v_0 = 0$, different drifts appear for different $v_0$. The larger the $|v_0|$, the faster the drift. Obviously, no matter how $v_0$ changes, the patterns of instantaneous shape remain the same. This means the tilt of dispersion does not affect ZB (which is the interference between inner states) but results in an obvious drift.

In order to better understand the wave packet dynamical properties, we calculate the analytical expression of the centroid motion. In Heisenberg picture, the time-dependent position operator reads

$$x(t) = \mathrm{e}^{\mathrm{i}\frac{H_{\mathrm{eff}}}{\hbar}t}x(0)\,\mathrm{e}^{-\mathrm{i}\frac{H_{\mathrm{eff}}}{\hbar}t}. \tag{10}$$

After plugging the Hamiltonian $H_{\mathrm{eff}}$ [(Eq. (5)] into the above expression, one can obtain

$$x(t) = x(0) + \alpha_x t + \beta_x t\left[\cos\left(\frac{2\tilde{E}t}{\hbar}\right) - 1\right] + \gamma_x \sin\left(\frac{2\tilde{E}t}{\hbar}\right), \tag{11}$$

where

$$\begin{aligned}
\alpha_x &= v_0 + \frac{v_x^2 q_x(v_x q_x \sigma_1 + m\sigma_3)}{\tilde{E}^2},\\
\beta_x &= \frac{\hbar}{2\tilde{E}^2\mathrm{i}}(v_x m\mathrm{i}\sigma_2),\\
\gamma_x &= \frac{\hbar}{2\tilde{E}^3}(v_x m^2\sigma_1 - v_x^2 q_x m\sigma_3),
\end{aligned} \tag{12}$$

with $\tilde{E} = \sqrt{v_x^2 q_x^2 + m^2}$. It can be seen clearly that $x(t)$ is a $2\times 2$ matrix. The first two terms in $x(t)$ account for classical kinematics, whereas the third and fourth terms denote the ZB effect. The frequency of ZB, which can be estimated as $\omega \sim 2|\tilde{E}|/\hbar = 2\sqrt{v_x^2 q_x^2 + m^2}/\hbar \sim 2|m|$, grows linearly with increasing $2|m|$. The same initial state [Eq. (9)] has been considered in the following formal logic derivation. The expression of $\bar{x}(t)$ can be obtained as

$$\begin{aligned}
\bar{x}(t) &= \langle\Psi_q|x(t)|\Psi_q\rangle\\
&= \frac{L}{\sqrt{\pi}}\int_{-\infty}^{\infty} A_x t + B_x\left[\cos\left(\frac{2\tilde{E}t}{\hbar}\right) - 1\right]\\
&\quad + C_x \sin\left(\frac{2\tilde{E}t}{\hbar}\right)\mathrm{e}^{-2L(q_x-q_0)^2}\,\mathrm{d}q_x.
\end{aligned} \tag{13}$$

For the case of $\Phi = \frac{1}{\sqrt{2}}(1,1)^{\mathrm{T}}$, the coefficients $A_x = v_0 + v_x^3 q_x^2/\tilde{E}^2$, $B_x = 0$, $C_x = \hbar v_x m^2/(2\tilde{E}^3)$. From the expression, one can find that there is no $v_0$ in ZB term, which means that the parameter $v_0$ does not affect the ZB effect at all. The centroid motions of atomic wavepacket $\bar{x}(t)$ are plotted in Fig. 3, the lines and symbols denote the analytical and numerical results, respectively. Figures 3(a) and 3(b) exhibit the centroid motion for different $v_0$ and $m$. Figures 3(c) and 3(d) show the corresponding frequency and amplitude of the ZB effect.

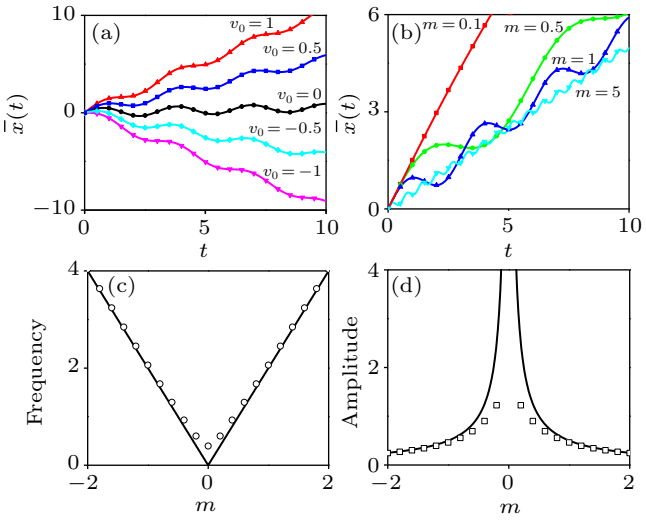



**Fig. 3.** Analytically (lines) and numerically (symbols) calculated ZB effect. The expectation value $\bar{x}(t)$ with different $v_0$ ($m$) is shown in (a) [(b)]. The corresponding frequency (c) and amplitude (d) of ZB with different $m$ are provided. Throughout the calculation, the width of the initial wavepacket $L = 2$ and effective fermi velocity $v_x = 1$.

Figure 3(a) reveals that the drift velocity increases with the increase of $v_0$ (from negative to positive), while the difference of $v_0$ does not affect the ZB effect at all. Since $\bar{x}(t)$ is the superposition of linear motion and periodic oscillation (ZB), one can obtain the same conclusion in the mathematical expressions [there is no $v_0$ in oscillation term ($\beta_x$ and $\gamma_x$) in Eq. (12)], which means ZB does not rely on the parameter $v_0$. The results of $\bar{x}(t)$ in Fig. 3(a) match the evolutions of the wavepacket (see Fig. 2) well, which is clear that $v_0$ is the parameter to drive a drift velocity of wave packet rather than ZB. From Fig. 3(b), one can see that the period and amplitude of ZB effect decrease with increasing $m$, which is in agreement with the analytical expression. To make it clearer, we plot the frequency and amplitude of ZB versus $m$ in Figs. 3(c) and 3(d). Symbols denote the numerical value by different $m$, while the lines correspond to the expect solution. Though the numerical results deviate the exact solution around $m = 0$, it works in most cases.

## 4. Momentum analysis

From Fig. 1(b), for $v_0 \neq 0$ (the tilted dispersion), there is a drift of atomic wavepacket. As we know, the wave vector $q_0$ denotes the initial velocity of the wavepacket, which also can provide a drift speed. Are they exactly the same thing? To find the answer, we comparatively study the effect of $v_0$ and $q_0$ and plot them in Fig. 4. Both of them result in a certain drift, whereas $q_0$ provides an additional effect on ZB. To further understand the distinction between $v_0$ and $q_0$, we do a momentum analysis to pinpoint the difference and reveal the underlying reason in the spectrum structure.[34] The corresponding momentum distributions $\Psi_\pm$ of positive and negative branches are shown in Fig. 5.

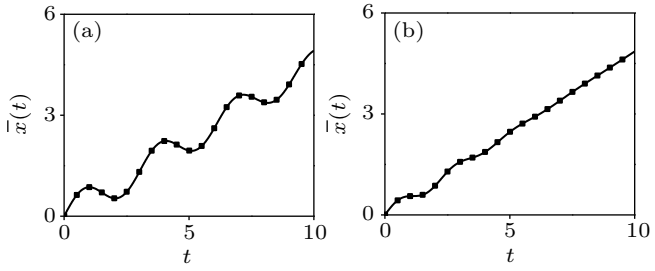



**Fig. 4.** The expectation value $\bar{x}(t)$ for the cases of (a) $v_0 = 0.5$ and (b) $q_0 = 0.5$. The lines (symbols) correspond to the exact solution (numerical results).

All square-integrable solution of the Dirac equation can be written in the form

$$\psi(x,t) = \int_{-\infty}^{\infty} \Big[\hat{\psi}_{\rm pos}(q_x) u_{\rm pos}(q_x;x,t) + \hat{\psi}_{\rm pos}(q_x) u_{\rm pos}(q_x;x,t)\Big] {\rm d}q_x. \quad (14)$$

The functions $\hat{\psi}_{\rm pos}$ and $\hat{\psi}_{\rm neg}$ can be determined from the Fourier transform $\hat{\psi}(q_x,0)$ of the initial function $\psi(x,0)$ by a projection in the positive or negative energy subspace. Numerical integration of Eq. (14) provides a method to compute the momentum analysis of free time evolution for an arbitrary initial wave packet. First, we calculate the momentum distribution of positive and negative-energy parts for $v_0 = -0.5, 0, 0.5$ to double check that the parameter $v_0$ cannot affect the interference of the inner state. Then, we set different initial wave vector $q_0 = -0.5, 0, 0.5$ and keep $v_0 = 0$ to calculate the momentum distribution once again. For the wave packet Eq. (8), figure 5 shows the momentum distributions of the parts with positive and negative energy, i.e., the functions $|\hat{\psi}_{\rm pos}(q_x)|^2$ and $|\hat{\psi}_{\rm neg}(q_x)|^2$. We see that the positive-energy part has its momentum distribution slightly shifted towards positive average momentum, whereas the negative-energy part has a negative average momentum. As is known to all, a positive average momentum means a positive average velocity for the positive-energy component of wave packet. However, a negative average momentum corresponds to a positive average velocity for a negative-energy component of wave packet. Then, one can see clearly that the whole wave packet in Figs. 5(a)–5(c) has a positive average velocity. Furthermore, the size of the overlap area between positive and negative-energy parts represents the intensity of ZB.

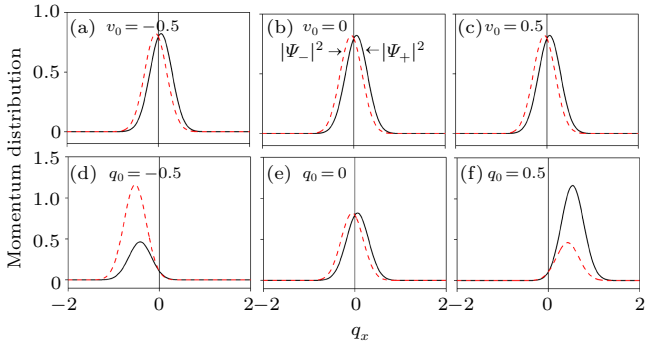



**Fig. 5.** Momentum distributions of the positive and negative energy parts of the wave packet: (a) $v_0 = -0.5$, (b) $v_0 = 0$, (c) $v_0 = 0.5$ with $q_0 = 0$; (d) $q_0 = -0.5$, (e) $q_0 = 0$, (f) $q_0 = 0.5$ with $v_0 = 0$.

As shown in Figs. 5(a)–5(c), no matter how the parameter $v_0$ changes, the shape of the momentum distribution remains unchanged, where the positive and negative parts show the same size with mirror symmetry. These momentum distributions are only determined by inner wavepackets' dynamics (ZB), so the corresponding patterns of ZB remain unchanged, which are the same as the case of $v_0 = 0$. From the result, we confirm that $v_0$ cannot affect the inner motion of wave packet again. As shown in Figs. 5(d)–5(f), there are different shapes of momentum distribution with different $q_0$. Notably, the overlap area with $q_0 \neq 0$ is less than that with $q_0 = 0$, which means that the intensity of inner states' interference (ZB effect) for $q_0 \neq 0$ is weaker than that for $q_0 = 0$. This result agrees with Fig. 4 well. Furthermore, by analyzing Figs. 5(d) and 5(f), we find that $q_0$ can only drive a positive velocity.

As we know, the slope of spectrum reflects the group velocity ($v_g = \partial E/\partial q_x$) of atomic wavepackets. The group velocity corresponds to the drift velocity of wave packet, so the tilting of spectrum can drive an obvious drift velocity rather than the effect on ZB. On the other hand, one of the key conditions of ZB effect is the energy gap. Different values of $q_0$ lead to different wavepacket centers in momentum space. Then, the atomic wavepackets will feel different gap widths of the same spectrum, so it can lead to different intensities of ZB. Therefore, the wave packet with $q_0 \neq 0, v_0 = 0$ is different from that with $q_0 = 0, v_0 \neq 0$.

## 5. Using quantum quench to realize component separation

The issue of statistical ensembles emerging in isolated quantum systems after a sudden perturbation, often referred to as quantum quench, has recently become a focal point of statistical physics research. For general spin-1/2 relativistic quasiparticles, the wave packet is composed of two components, i.e., spin-up ($|\uparrow\rangle$) and spin-down ($|\downarrow\rangle$) states. The atomic wavepacket satisfies the principle of linear superposition, i.e., $|\Psi\rangle = A\,|\uparrow\rangle + B\,|\downarrow\rangle$, where $A$ and $B$ are coupling coefficients. However, a mixed initial state is not easy to separate completely in table-top experiments. Note that, the mono-component $|\uparrow\rangle$ ($|\downarrow\rangle$) can not exist in a certain local position steadily for a long time because it usually diffuses rapidly when the harmonic trap is tuned off. In order to realize a stable single component wavepacket, we propose a quantum quench process and use the feature of parameter $v_0$ to realize component separation. First, one can prepare an initial state [Bose–Einstein condensates, or a cold atomic ensemble] and transfer it into SSH lattice. In the next step, let the atomic cloud evolve satisfying the Hamiltonian of the standard SSH model. After a certain duration, we tune on the NNN hopping by controlling the lasers. Then, the atomic cloud would change into another Hamiltonian with tilted spectrum. Here, we study the effect of the value of $v_0$ and evolution of wavepacket in Hamiltonian [Eq. (5)], then we let wavepacket evolve in one Hamiltonian, after a while in another Hamiltonian. We summarize and plot the relation between $k_0$ and $v_0$ to obtain a stably mono-component atomic wavepacket. The inset of Fig. 6 shows the atomic gases evolution with the parameters under the condition of red star.

It is clear to see that the wavepacket separates into $|\uparrow\rangle$ and $|\downarrow\rangle$. Notably, $|\uparrow\rangle$ can exist in local position steadily for a long time after a sudden $v_0$ quench. In short, by introducing quantum quench of $v_0$ during the process of wavepacket's evolution, a pure and stable spin-up component can be observed.

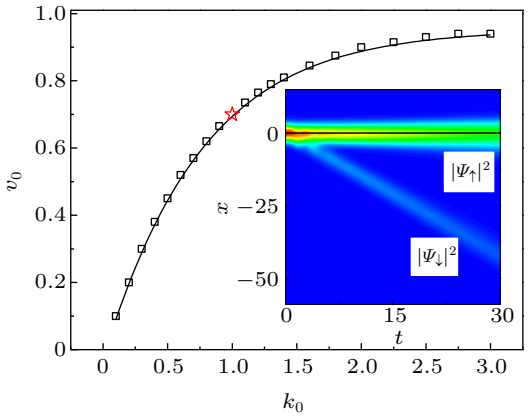



**Fig. 6.** The relationship of $q_0$ and $v_0$ for a stable single pure component wave packet. Insert: Visualized wavepacket for the condition of red star. Through the numerical calculation, the other parameters $L = 2$, $q_0 = 0.5$, $m = 1$, and $v_x = 1$.

## 6. Conclusion

In summary, we have explored 1D relativistic quasiparticles' dynamics in an optical lattice. From SSH model with the NNN hopping, we find that the low energy expansion spectrum gets tilted. By manipulating the tunable parameter $v_0$, we calculate the evolution of quasiparticles and provide a well-visualized picture for quasiparticles' wave packet. The results show that the wavepacket evolves at different velocities with an obvious period oscillation (ZB), which corresponds to the parameter $v_0$. Furthermore, we deduce the analytical expression for the exceptional value of atomic wavepacket versus time. The analytical results match the numerical ones well. We notice that $v_0$ merely drives a drift of wavepacket instead of an effect of inner states' interference. The amplitude and frequency of ZB effect are determined by $m$ rather than $v_0$. Further study shows that the frequency increases with an increasing $m$, whereas the amplitude decreases with that. Besides, to distinguish the $v_0$ (tilted spectrum) effect from $k_0$ (initial velocity), we analyze the momentum distributions of the positive and negative energy parts of the atomic wavepacket. The results show while $v_0$ can drive a drift of atomic, it can not replace the initial wave vector $k_0$. Finally, we propose a quench cold atomic lattice system to realize a pure and stable mono-component wavepacket. We hope our work will benefit the research of relativistic quasiparticles and related physics in cold atomic lattice systems.

## Appendix A: The derivation process detail from tight-binding model to continuous Hamiltonian

$$H = \sum_{n=1}^{N} \Big\{ \mathrm{e}^{\mathrm{i}\frac{\pi}{2}} t_1 (a_n^\dagger a_{n+1} + b_n^\dagger b_{n+1}) + t_2(1+\alpha) a_{,n}^\dagger b_n + t_2(1-\alpha) a_{n+1}^\dagger b_n + \mathrm{h.c.} \Big\}. \quad \text{(A1)}$$

Performing the Fourier transformation

$$a_n = \sum_{k_x} \mathrm{e}^{\mathrm{i}k_x na} a_{k_x}, \tag{A2}$$

$$b_n = \sum_{k_x} \mathrm{e}^{\mathrm{i}k_x na} b_{k_x}. \tag{A3}$$

Introducing the spinor

$$\psi_{k_x} = \begin{pmatrix} a_{k_x} \\ b_{k_x} \end{pmatrix}. \tag{A4}$$

The first hopping term

$$\begin{aligned}
&\mathrm{e}^{\mathrm{i}\frac{\pi}{2}} t_1 \sum_{n=1}^{N} (a_n^\dagger a_{n+1} + b_n^\dagger b_{n+1}) + \text{h.c.} \\
&= t_1 \sum_{n=1}^{N} \left( \mathrm{i} a_n^\dagger a_{n+1} - \mathrm{i} a_{n+1}^\dagger a_n + \mathrm{i} b_n^\dagger b_{n+1} - \mathrm{i} b_{n+1}^\dagger b_n \right) \\
&= \mathrm{i}t_1 \sum_{k_x} \left( a_{k_x}^\dagger \mathrm{e}^{-\mathrm{i}k_x na} a_{k_x} \mathrm{e}^{\mathrm{i}k_x na} \mathrm{e}^{\mathrm{i}k_x a} - a_{k_x}^\dagger \mathrm{e}^{-\mathrm{i}k_x na} a_{k_x} \mathrm{e}^{\mathrm{i}k_x na} \mathrm{e}^{-\mathrm{i}k_x a} \right. \\
&\quad \left. + b_{k_x}^\dagger \mathrm{e}^{-\mathrm{i}k_x na} b_{k_x} \mathrm{e}^{\mathrm{i}k_x na} \mathrm{e}^{\mathrm{i}k_x a} - b_{k_x}^\dagger \mathrm{e}^{-\mathrm{i}k_x na} b_{k_x} \mathrm{e}^{\mathrm{i}k_x na} \mathrm{e}^{-\mathrm{i}k_x a} \right) \\
&= \mathrm{i}t_1 \sum_{k_x} \left( a_{k_x}^\dagger a_{k_x} \mathrm{e}^{\mathrm{i}k_x} - a_{k_x}^\dagger a_{k_x} \mathrm{e}^{-\mathrm{i}k_x} + b_{k_x}^\dagger b_{k_x} \mathrm{e}^{\mathrm{i}k_x} - b_{k_x}^\dagger b_{k_x} \mathrm{e}^{-\mathrm{i}k_x} \right) \\
&= \mathrm{i}t_1 \sum_{k_x} \left( a_{k_x}^\dagger a_{k_x} (\mathrm{e}^{\mathrm{i}k_x} - \mathrm{e}^{-\mathrm{i}k_x}) + b_{k_x}^\dagger b_{k_x} (\mathrm{e}^{\mathrm{i}k_x} - \mathrm{e}^{-\mathrm{i}k_x}) \right) \\
&= -2t_1 \sum_{k_x} \left( a_{k_x}^\dagger a_{k_x} \sin k_x + b_{k_x}^\dagger b_{k_x} \sin k_x \right) \\
&= -2t_1 \sum_{k_x} \psi_{k_x}^\dagger (\sin k_x \sigma_0) \psi_{k_x}.
\end{aligned} \tag{A5}$$

The second and third hopping terms

$$\begin{aligned}
&\sum_{n=1}^{N} t_2(1+\alpha) a_n^\dagger b_n + t_2(1-\alpha) a_{n+1}^\dagger b_n + \text{h.c.} \\
&= t_2(1+\alpha) \sum_{k_x} \left( a_{k_x}^\dagger b_{k_x} + b_{k_x}^\dagger a_{k_x} \right) \\
&\quad + t_2(1-\alpha) \sum_{k_x} \left( a_{k_x}^\dagger b_{k_x} \mathrm{e}^{-\mathrm{i}k_x} + b_{k_x}^\dagger a_{k_x} \mathrm{e}^{\mathrm{i}k_x} \right) \\
&= t_2(1+\alpha) \sum_{k_x} (a_{k_x}^\dagger b_{k_x} + b_{k_x}^\dagger a_{k_x}) \\
&\quad + t_2(1-\alpha) \sum_{k_x} \left( a_{k_x}^\dagger b_{k_x} (\cos k_x - \mathrm{i} \sin k_x) \right. \\
&\quad \left. + b_{k_x}^\dagger a_{k_x} (\cos k_x + \mathrm{i} \sin k_x) \right) \\
&= \sum_{k_x} \psi_{k_x}^\dagger \left[ (t_2(1+\alpha) + t_2(1-\alpha) \cos k_x) \sigma_1 \right. \\
&\quad \left. + t_2(1-\alpha) \sin k_x \sigma_2 \right] \psi_{k_x}.
\end{aligned} \tag{A6}$$

Under a transformation, $\sigma_1 \to \sigma_3$, $\sigma_2 \to \sigma_1$, and $\sigma_3 \to \sigma_2$, and $k_x \to k_x + \pi$, it is reduced to

$$\begin{aligned}
H = \sum_{k_x} \psi_{k_x}^\dagger \Big[ & 2t_1 \sin k_x \sigma_0 + (-t_2(1-\alpha) \sin k_x) \sigma_1 \\
& + \left( 2\alpha t_2 + 2t_2(1-\alpha) \sin^2 \frac{k_x}{2} \right) \sigma_3 \Big] \psi_{k_x}.
\end{aligned} \tag{A7}$$

For simplicity, leaving out high-order term and making $2t_1 = v_0$, $-t_2(1-\alpha) = v_x$, $2\alpha t_2 = m$, one can obtain the low-order Hamiltonian in a compact form

$$H = \sum_{k_x} \psi_{k_x}^\dagger (v_0 \sin k_x \sigma_0 + v_x \sin k_x \sigma_1 + mc^2 \sigma_3) \psi_{k_x}. \tag{A8}$$

Then we obtain the Bloch Hamiltonian

$$H_k = v_0 \sin k_x \sigma_0 + v_x \sin k_x \sigma_1 + mc^2 \sigma_3. \tag{A9}$$

## Appendix B: Symmetry of Bloch Hamiltonian

Time reversal is a transformation that reverses the arrow of time:

$$T : t \to -t, \tag{B1}$$

$$T \hat{x} T^{-1} = x, \quad T k_x T^{-1} = -k_x. \tag{B2}$$

So,

$$\begin{aligned}
T H_k T^{-1} &= T \left( v_0 \sin k_x \sigma_0 + v_x \sin k_x \sigma_1 + mc^2 \sigma_3 \right) T^{-1} \\
&= v_0 \sin -k_x \sigma_0 + v_x \sin -k_x \sigma_1 + mc^2 \sigma_3 \\
&\neq H_k.
\end{aligned} \tag{B3}$$

Thus, the time-reversal symmetry of the Bloch Hamiltonian is broken.

Inversion symmetry is a transformation that reverses the arrow of space:

$$P : x \to -x, \tag{B4}$$

$$P \hat{x} P^{-1} = -x, \quad P k_x P^{-1} = -k_x. \tag{B5}$$

So,

$$\begin{aligned}
P H_k P^{-1} &= P(v_0 \sin k_x \sigma_0 + v_x \sin k_x \sigma_1 + mc^2 \sigma_3) P^{-1} \\
&= v_0 \sin -k_x \sigma_0 + v_x \sin -k_x \sigma_1 + mc^2 \sigma_3 \\
&\neq H_k.
\end{aligned} \tag{B6}$$

Thus, the inversion symmetry of the Bloch Hamiltonian is broken.

The combining $PT$ symmetry is transformation that reverses the arrow of both time and space:

$$PT : t \to -t, \ \ x \to -x, \tag{B7}$$

$$PT \hat{x} PT^{-1} = -x, \ \ PT k_x PT^{-1} = k_x. \tag{B8}$$

So,

$$\begin{aligned}
PT H_k PT^{-1} &= PT(v_0 \sin k_x \sigma_0 + v_x \sin k_x \sigma_1 + mc^2 \sigma_3) PT^{-1} \\
&= v_0 \sin k_x \sigma_0 + v_x \sin k_x \sigma_1 + mc^2 \sigma_3 \\
&= H_k.
\end{aligned} \tag{B9}$$

Thus, the combining $PT$ symmetry of the Bloch Hamiltonian remains intact.

## References


[1] Schrödinger E 1930 *Sizungsber. Preuss. Akad. Wiss. Phys. Math. Kl.* **24** 418

[2] Gerritsma R, Kirchmair G, Zähringer F, *et al.* 2010 *Nature* **463** 68

[3] Barut A O and Bracken A J 1981 *Phys. Rev. D* **23** 2454

[4] Schliemann J, Loss D and Westervelt R M 2005 *Phys. Rev. Lett.* **94** 206801

[5] Katsnelson M I 2006 *Eur. Phys. J. B* **51** 157
[6] Zhang X D 2008 *Phys. Rev. Lett.* **100** 113903
[7] Vaishnav J Y and Clark C W 2008 *Phys. Rev. Lett.* **100** 153002
[8] Zawadzki W and Rusin T M 2011 *J. Phys.: Condens. Matter* **23** 143201
[9] Li Z, Wang H Q, Zhang D W, Zhu S L and Xing D Y 2016 *Phys. Rev. A* **94** 043617
[10] Huang T Y, Ma T and Wang L 2018 *J. Phys.: Condens. Matter* **30** 245501
[11] Zhang D W, Zhu Y Q, Zhao Y X, Yan H and Zhu S L 2018 *Adv. Phys.* **67** 253
[12] Su W P, Schrieffer J R and Heeger A J 1979 *Phys. Rev. Lett.* **42** 1698
[13] Meier E J, An F A and Gadway B 2016 *Nat. Commun.* **7** 13986
[14] Schomerus H 2013 *Opt. Lett.* **38** 1912
[15] Engelhardt G, Benito M, Platero G and Brandes T 2017 *Phys. Rev. Lett.* **118** 197702
[16] Zhu S L, Wang B G and Duan L M 2007 *Phys. Rev. Lett.* **98** 260402
[17] Zhu S L, Zhang D W and Wang Z D 2009 *Phys. Rev. Lett.* **102** 210403
[18] Zhu S L, Shao L B, Wang Z D and Duan L M 2011 *Phys. Rev. Lett.* **106** 100404
[19] Cooper N R, Dalibard J and Spielman I B 2019 *Rev. Mod. Phys.* **91** 015005
[20] Lewenstein M, Sanpera A, Ahufinger V, Damski B, De A S and Sen U 2007 *Adv. Phys.* **56** 243
[21] Dalibard J, Gerbier F, Juzeliūnas G and Öhberg P 2011 *Rev. Mod. Phys.* **83** 1523
[22] Goldman N, Juzeliūnas G, Öhberg P and Spielman I B 2014 *Rep. Prog. Phys.* **77** 126401
[23] Islam R, Senko C, Campbell W C, *et al.* 2013 *Science* **340** 583
[24] Zhao W L, Gong J B, Wang W G, Casati G, Liu J and Fu L B 2016 *Phys. Rev. A* **94** 053631
[25] Dou F Q, Cao H, Liu J and Fu L B 2016 *Phys. Rev. A* **93** 043419
[26] Zhao W L, Wang J Z, Xiaohui Wang X H and Tong P Q 2019 *Phys. Rev. E* **99** 042201
[27] Li S C, Fu L B and Liu J 2018 *Phys. Rev. A* **98** 013601
[28] Dou F Q, Liu J and Fu L B 2018 *Phys. Rev. A* **98** 022102
[29] Li Z, Cao H and Fu L B 2015 *Phys. Rev. A* **91** 023623
[30] Hu X D, Huang Y L, Shen X, Liao K Y and Li Z 2019 *Phys. Lett. A* **383** 125982
[31] Shen X and Li Z 2018 *Phys. Rev. A* **97** 01360
[32] Shen X, Wang F D, Li Z and Wu Z G 2019 *Phys. Rev. A* **100** 062514
[33] Shen X, Zhang D W, Yan H, Li Z and Zhu S L 2020 *Phys. Rev. Research* **2** 013037
[34] Thaller B 2004 arXiv quant-ph/0409079